PCCP

PAPER

View Article Online
View Journal | View Issue

Cite this: *Phys. Chem. Chem. Phys.*, 2025, **27**, 6056

Molecular insight into the dynamics at the lithium-containing ionic liquid/gold film electrode interface using electrochemical attenuated total reflection spectroscopies†

Tomonori Kakinoki, *[a] Akihito Imanishi, [a] Shinji Kondou, [a] Ichiro Tanabe [b] and Ken-ichi Fukui *[a]

Received 24th December 2024,
Accepted 25th February 2025

DOI: 10.1039/d4cp04831h

rsc.li/pccp

The spectral response at the interface between lithium-containing 1-ethyl-3-methyl-imidazolium bis(trifluoromethanesulfonyl)imide (EMIM-TFSI) and a gold electrode was investigated using electrochemical attenuated total reflection spectroscopy (EC-ATR) in the far-ultraviolet and infrared regions. At a negatively charged Au electrode within the cathodic limit, an increase in the EMIM cation signal and a decrease in the TFSI anion signal were observed for neat EMIM-TFSI, indicating the normal replacement of the TFSI anions by the EMIM cations. In contrast, an apparent decrease in the EMIM cation signal and an increase in the TFSI anion signal were observed, suggesting the replacement of the EMIM cation with a Li^+ cation coordinated with TFSI anions. The ATR spectral responses were reversible in the electrode potential cycles, likely due to diffusion perpendicular to the electrode or the reorientation of the interfacial ionic liquid components. The surface-stabilized Li^+ ions coordinated by the TFSI anions at the negatively charged Au electrode may restrict the direct interaction of the EMIM cation with the electrode, thereby reducing the reduction rate of the EMIM cation, and extending the cathodic limit upon the addition of the Li salt.

Introduction

Lithium-ion (Li^+) batteries are among the most successfully developed electrochemical devices and are currently used worldwide. One of the serious problems with current Li^+ batteries is the flammability of the organic electrolyte. Numerous attempts have been made to address this issue;[1,2] however, a fundamental solution has yet to be achieved. A straightforward approach involves replacing the flammable electrolyte with a non-flammable alternative,[3] such as room-temperature ionic liquids (ILs). ILs have advantages other than non-flammability, such as wide electrochemical windows and low vapor pressure.[4]

ILs can be considered high-density electrolytes, thus strengthening electrostatic interactions even in the bulk phase. Nanodomain structures that separate polar part and non-polar part parts were observed in the bulk.[5] The properties of ILs at solid interfaces are strongly affected by the nature of the solid materials. From force spectra measurements using atomic force microscopy (AFM),[6,7] and molecular dynamics (MD) calculations,[8,9] ILs generally exhibit a layered structure, comprising units with a thickness equivalent to the cation–anion pair of the IL at solid interfaces. The rigidity of the layers and diffusion of cations and anions within these layers vary depending on the choice of the ILs and solids.

The electric double-layer (EDL) structure of ILs at electrode interfaces is also unique compared to the typical structure assumed for dilute electrolyte solutions.[10] The EDL structure changes while maintaining the character of the layered structure. Force curve measurements at the electrode interfaces revealed that the rigidity of the layered structure increased due to enhanced electrostatic interactions at the interface induced by electrode potential application.[11,12] The conventional view of an anion-rich layer at a positively charged electrode and a cation-rich layer at a negatively charged electrode does not generally apply to ILs.[9,13,14] Hysteresis is often observed in the electrode-potential response of ILs, and the dynamics of cations and anions at electrified interfaces have been examined using interface-sensitive spectroscopic methods.[15,16] To further explore the properties of ILs as electrolytes, we conducted an interface analysis of a lithium-containing system.

The cathodic limit of the electrochemical window of ILs was significantly shifted to a more negative potential by the addition of lithium salts. Matsumoto[17] demonstrated an extension

[a] *Department of Materials Engineering Science, Graduate School of Engineering Science, Osaka University, 1-3 Machikaneyama, Toyonaka, Osaka 560-8531, Japan. E-mail: fukui.ken-ichi.es@osaka-u.ac.jp*
[b] *College of Science Department of Chemistry, Graduate School of Science, Rikkyo University, 3-34-1, Nishiikebukuro, Toshima, Tokyo 171-0021, Japan*

† Electronic supplementary information (ESI) available. See DOI: https://doi.org/10.1039/d4cp04831h

of the cathodic limit of 1-ethyl-3-methyl-imidazolium bis(trifluoromethanesulfonyl)imide (EMIM-TFSI) on a Pt electrode by adding Li-TFSI. Similar shifts due to the addition of Li salts have also been reported in another system.[18–21] This phenomenon is often attributed to a kinetic effect, where the access of the IL cations and anions to the electrode is restricted. For instance, a spectroscopic investigation concerning this matter involved analyzing the potential response of Li-containing EMIM-bis(fluorosulfonyl)azanide (FSA) on a Pt electrode using sum frequency generation spectroscopy.[22] The analysis suggested that the strong interaction of Li^+ with FSI anchors the anion to the negatively charged electrode and prevents adsorption and reduction of the EMIM cation on the Pt electrode. Therefore, it is possible that changes in the interfacial layer structure directly affect the cathodic limit extension.

This study aimed to understand the microscopic dynamics of the electrochemical interface of a Li-containing IL (LIL). Attenuated total reflection (ATR) spectroscopy is an interface-sensitive analysis technique that utilizes exponentially decaying light (evanescent waves) from the interface where the total reflection of probe light occurs. In particular, the short penetration depth of the evanescent wave in the far ultraviolet (FUV) region enables the detection of spectra containing information near the reflection interface.[23,24] Recently, we have developed electrochemical ATR-FUV spectroscopy.[25] By analyzing the potential response of 1-butyl-3-methylimidazolium iodide (BMIM-I) on a comb-shaped Pt electrode, we discovered that intermolecular electronic transitions between iodide ions and BMIM cations near the electrode were notably enhanced by a positive charge application to the electrode. Thus, this analytical approach can identify signals that characterize electrochemical interfaces. In this study, we explored the molecular dynamics of lithium-containing EMIM-TFSI on a negatively charged Au electrode using electrochemical ATR absorbance spectroscopies in FUV (EC-ATR-FUV) and IR (EC-ATR-IR) regions.

Method

Sample preparation

EMIM-TFSI (>98.0%) was used as an IL, and Li-TFSI (>98.0%) served as the Li^+ solute, both obtained from Tokyo Chemical Industry Corporation. The IL was preheated under vacuum just before use (100 °C and 10^{-3} Pa for 24 h) to eliminate water and gaseous impurities. The Li^+ concentration in the LIL solution was adjusted to approximately 0.6 mol kg^{-1} (corresponding molar ratio Li-TFSI : EMIM-TFSI = 3 : 13), except for experiments involving Li^+ concentration dependent ATR-FUV spectra.

The internal optical elements for the ATR measurements were purchased from Pier Optics Corporation. Sapphire and silicon internal prisms were used for FUV and IR spectroscopy, respectively. Gold thin films (less than 10 nm thick for the FUV spectroscopy, and approximately 20 nm thick for the IR spectroscopy) were deposited under vacuum (10^{-4} Pa) on the ATR prisms and utilized as the working electrodes for the electrochemical measurements. The Au thin films exhibited sufficient electrical conductivity with the thickness being adequate for signal detection on the electrolyte side.

Electrochemical ATR-FUV spectroscopy

Electrochemical ATR-FUV (EC-ATR-FUV) spectroscopy measurements were conducted using a custom-built system (Fig. 1), as described in previous reports.[24,25] The ATR-FUV spectrometer (BUNKOUKEIKI Corporation) was utilized for measurements in the wavelength range of 160–250 nm at an incident angle of 70°. The interior of the spectrometer was purged with dry nitrogen gas to eliminate the absorption of oxygen and moisture in ambient air. The electrochemical potential of the working electrode was regulated using a three-electrode system equipped with a potentiostat (HSV-110, HOKUTO DENKO Corporation). A platinum mesh and a platinum rod served as the counter and reference electrodes, respectively and independently measured redox peak of ferrocene added to the LIL solution was used as the potential reference (*vs.* Fc/Fc^+). The spectral scan speed was set at 150 nm min^{-1}. For the EC-ATR-FUV measurements, the sweeping rate of the electrode potential was maintained at a slow rate of 40 mV min^{-1}, and cyclic voltammetry (CV) was conducted simultaneously. Spectral scans were performed at every 0.1 V interval.

Time-dependent density functional theory calculations

Time-dependent density functional theory (TD-DFT) calculations were conducted to identify the absorption peaks in the experimental ATR-FUV spectra. The Gaussian16 program was employed for calculations. Following the construction of frame structures for the EMIM cation and TFSI anion, the input structures were energetically optimized. In the calculation of the ground state, the B3LYP functional and 6-311G(d) basis set were used for the cation, while the 6-311G+(d) basis set was applied for the anion. The charge number and state were specified as +1 and singlet for the EMIM cation and −1 and singlet for the TFSI anion. Excited electronic states were calculated from the ground states using TD-DFT, with the CAM-B3LYP functional and 6-311G(d) and 6-311G+(d) basis

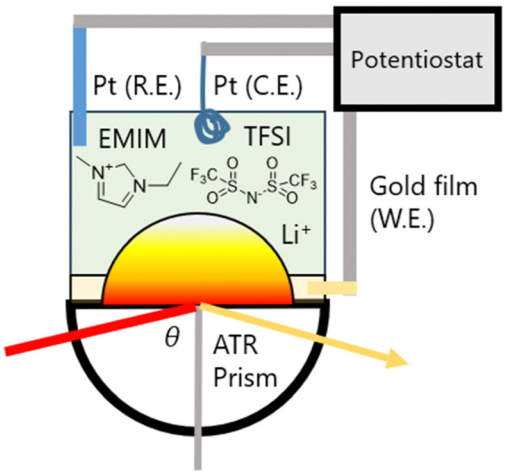

Fig. 1 Schematic of the experimental setup for EC-ATR-FUV measurements.

sets for the cations and anions, respectively. The oscillation strength was determined by the matrix of wave functions of the electronic states. A Gaussian function with a standard deviation of 0.2 eV was applied to the calculated oscillation strength to replicate absorption spectra.

Electrochemical ATR-IR spectroscopy

Electrochemical ATR-IR (EC-ATR-IR) spectroscopy measurements were conducted using a custom-built system shown in Fig. 1.[26] The cell, constructed from polyether ether ketone, was attached to a PIKE Technologies VeeMAX III angle-variable specular reflection accessory. The Fourier-transform infrared (FT-IR) spectrometer (Vertex70, Bruker Inc.) was used in the wavenumber range of 900–1500 cm^{-1} at an incident angle of 62°. The spectra obtained through these analyses are presented without any smoothing. The electrochemical potential of the working electrode was regulated *via* a three-electrode system using the potentiostat (HSV-110). The counter and reference electrodes were platinum mesh and rod, respectively. FT-IR spectra were measured at a resolution of 4 cm^{-1}, an accumulation count of 128 and a sampling rate of 80 kHz with a liquid-N_2-cooled MCT detector, ensuring stable conditions for single-spectrum measurements. The electrode potential sweep rate was maintained at a slow rate of 50 mV min^{-1}, with CV performed simultaneously. The difference in the measurement depths for the IR and FUV regions is detailed in the ESI† (S1.2).

Results and discussion

Extension of the cathodic limit of the electrochemical window with the Li^+ addition

The comparison of the cathodic limits of the electrochemical windows of the neat IL and the LIL is illustrated in Fig. 2(a). In the LIL, a pair of double peaks emerges within the range of −3.0 to −3.4 V, representing the redox peak of Li^+. The cathodic limit for the LIL, defined as the potential where the reduction current significantly increases was negatively shifted by approximately 0.5 V at the value of 50 μA cm^{-2}. The expansion of the cathodic limit through the addition of lithium salts has been repeatedly reported in previous studies and was attributed to the suppression of electrolyte decomposition.[19] However, a comprehensive molecular explanation for the phenomenon remains elusive. We hypothesized that different compositions and local structures of the constituent ions in the EDL layer region at potentials higher than the apparent onset of electrolyte decomposition are crucial for elucidating the limit expansion. Therefore, we studied the interface dynamics of the LIL electrolytes using interfacial spectroscopic methods, especially within the potential range of +1.5 to −2.5 V *vs.* Fc/Fc^+.

ATR-FUV spectra peak assignments

Fig. 3(a) shows the ATR-FUV absorbance spectra of neat EMIM-TFSI and LIL solutions with varying Li^+ concentrations using an ATR prism without an Au thin film. Two distinct peaks appear around 170 and 210 nm, which remain consistent regardless of the Li^+ concentration. These peaks were assigned to the intramolecular electronic transition for the EMIM cation.[27,28] As detailed in the ESI† (S1.1), a spectral simulation was conducted based on the Fresnel equations of the interface using optical parameters derived from the optical transformation method adapted for the ATR spectrum of neat EMIM-TFSI in Fig. 3(a).

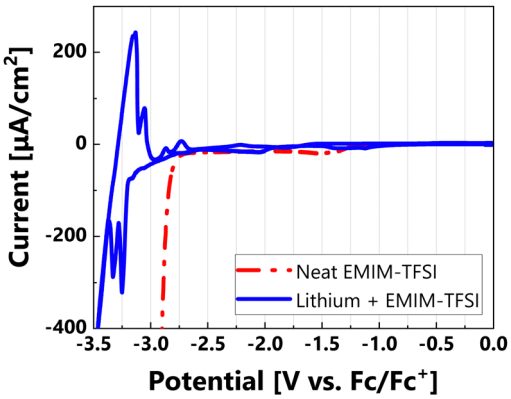

Fig. 2 CV curves for EMIM-TFSI with lithium (LIL, blue solid line) and without lithium (neat IL, red dash line) in the potential range of 0 to −3.4 V *vs.* Fc/Fc^+, measured at a sweep rate of 0.66 mV s^{-1}.

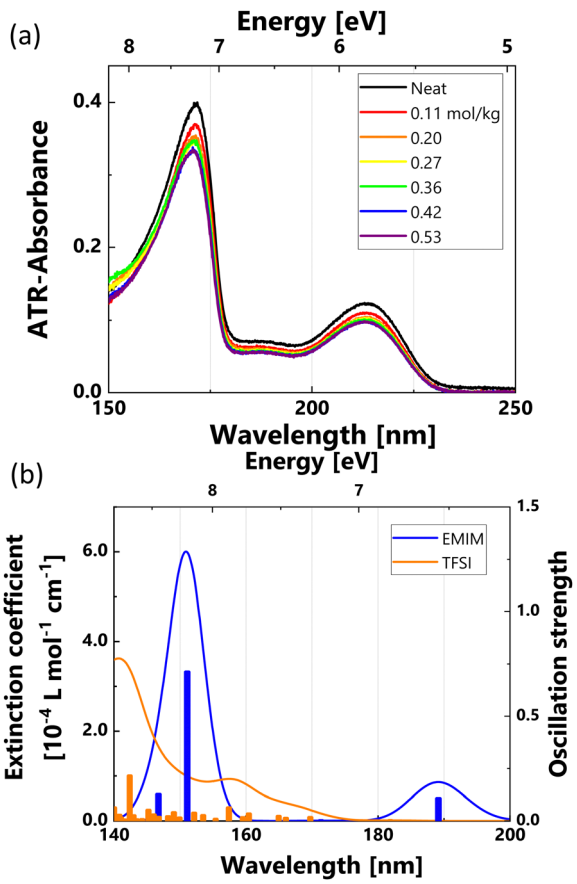

Fig. 3 (a) ATR-FUV spectra of neat EMIM-TFSI and LIL solutions with varying lithium concentrations, measured using an ATR prism without an Au thin film. (b) Calculated vertical transitions and absorption spectra for a single EMIM cation and a single TFSI anion, respectively.

The transformed extinction coefficient shown in Fig. S1(b) (ESI†) exhibits good consistency with the experimental transmission spectrum of EMIM-TFSI in Fig. S2 (ESI†), showing the major peaks at 164 and 210 nm, slightly shorter wavelength than the inherent ATR spectrum as generally observed (ESI†). The extinction coefficient estimated from the oscillation strength obtained by TD-DFT calculations for a single EMIM cation and a single TFSI anion in Fig. 3(b). The peak ratio and the peak separation of the major two peaks originating from the EMIM cation absorption almost coincide with those of Fig. S1(b) (ESI†) and Fig. 3(a), although the both peak positions are shifted by about 20 nm for the shorter wavelength side. The analysis in Fig. 3(b) confirms that TFSI anion absorbance predominates between the two absorption peaks (160–180 nm region in Fig. 3(b)) of the EMIM cation. Therefore, the TFSI anion is expected to make a more significant contribution to the absorbance in the 180–200 nm region in Fig. 3(a).

EC-ATR-FUV spectra at the interface between the Au electrode and neat EMIM-TFSI

To evaluate the effects of Li^+ addition, a control experiment was conducted using neat EMIM-TFSI. EC-ATR-FUV spectra of neat IL acquired at various potentials from 0 to −2.3 V *vs.* Fc/Fc^+ (more positive than the cathodic limit) are shown in Fig. 4(a). The spectrum of the Au electrode without the IL electrolyte served as the background spectrum. As detailed in the ESI† (S1.1), a spectral simulation was conducted based on the Fresnel equations of the electrode interface. The observed increase in slope toward longer wavelengths was primarily stemmed from the absorption of the Au film.

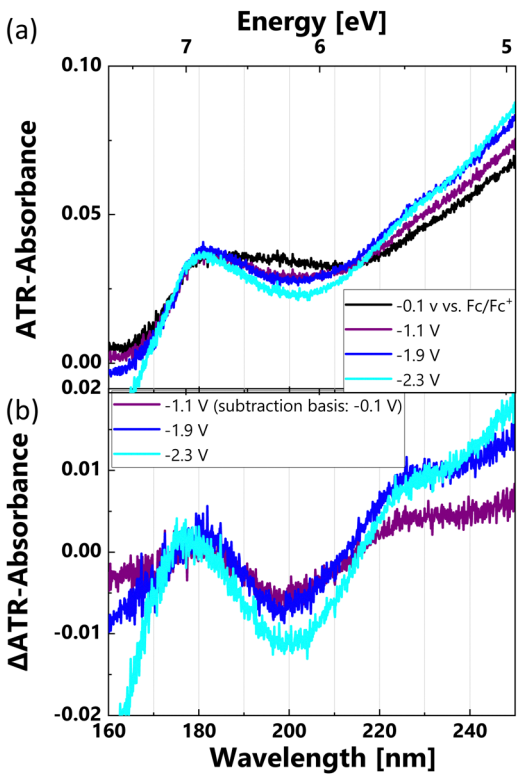

Fig. 4 (a) EC-ATR-FUV spectra of the interface in neat Il solution during the first cycle within the potential range of −2.3 to −0.1 V *vs.* Fc/Fc^+. (b) Difference spectra derived from (a), highlighting changes in the interface states.

When a negative electrode potential was applied to the Au electrode, a slight increase in absorption at 176 nm and a noticeable decrease in absorption at 190–210 nm were observed. This difference is more evident in the spectra shown in Fig. 4(b). Based on the peak assignment noted above, the absorption at 176 nm corresponds to the main absorption peak of the EMIM cation, while the absorption at 190–210 nm range originates from absorption of the TFSI anion. It is noteworthy that only a negligible current flows in this potential range as indicated by the concurrently recorded current–voltage curve (Fig. S6) in the ESI.† These findings strongly indicate that the apparent decrease in absorption around 200 nm resulted from the departure of TFSI anions at the interface due to electrostatic repulsion against the negatively charged Au electrode. Additionally, the slight increase in absorption at 176 nm was attributed to the realignment of the EMIM cations at the interface to conform to the Au electrode, effectively neutralizing the negative charge of the electrode while occupying the voids of the departing TFSI anions. These behaviors in pure IL systems have been consistently documented in previous papers.[9,16]

EC-ATR-FUV and EC-ATR-IR spectra at the interface between the Au electrode and Li-containing EMIM-TFSI

EC-ATR-FUV spectra of the LIL solution (0.6 mol kg^{-1}) at various potentials ranging from −2.2 to +1.5 V *vs.* Fc/Fc^+ are shown in Fig. 5(a). The background spectrum was obtained from the Au electrode without the LIL electrolyte. The simultaneously measured CV curve shown in Fig. 5(c) exhibited the same trend as the CV curve of the LIL in Fig. 2, indicating that the potential region for the spectral measurements was more positive than the large Li^+ redox peaks.

During the negative-going potential scan from −0.1 V, no significant spectral change was observed until the potential reached −1.5 V. As shown in the spectra of Fig. 5(a) and the red difference spectrum in Fig. 5(b), a noticeable decrease in absorption at 176 nm and a smaller increase in absorption in the 190–220 nm region were observed in the spectrum at −2.2 V. The absorption at 176 nm corresponds to the larger absorption peak of the EMIM cation, while the absorption at 190–220 nm region is attributed to the TFSI anion. Therefore, the changes at −2.2 V indicate a decrease in EMIM cation absorption and increase in TFSI absorption, representing an opposite trend compared to the spectra of neat EMIM-TFSI in Fig. 4(a) and (b).

During the positive-going potential scan after reversing at −2.2 V, the decrease in EMIM cation absorption persisted until −1.2 V, while TFSI absorption did not increase but rather decreased. The delayed spectral change is probably due to the sluggish response of the LIL electrolyte, even at a slow scanning rate of 40 mV min^{-1}. The reduction in the EMIM cation absorption partially recovered at +0.6 V after surpassing the initial potential, significantly recovered at the second reversal potential of +1.5 V, and finally a similar spectrum was observed

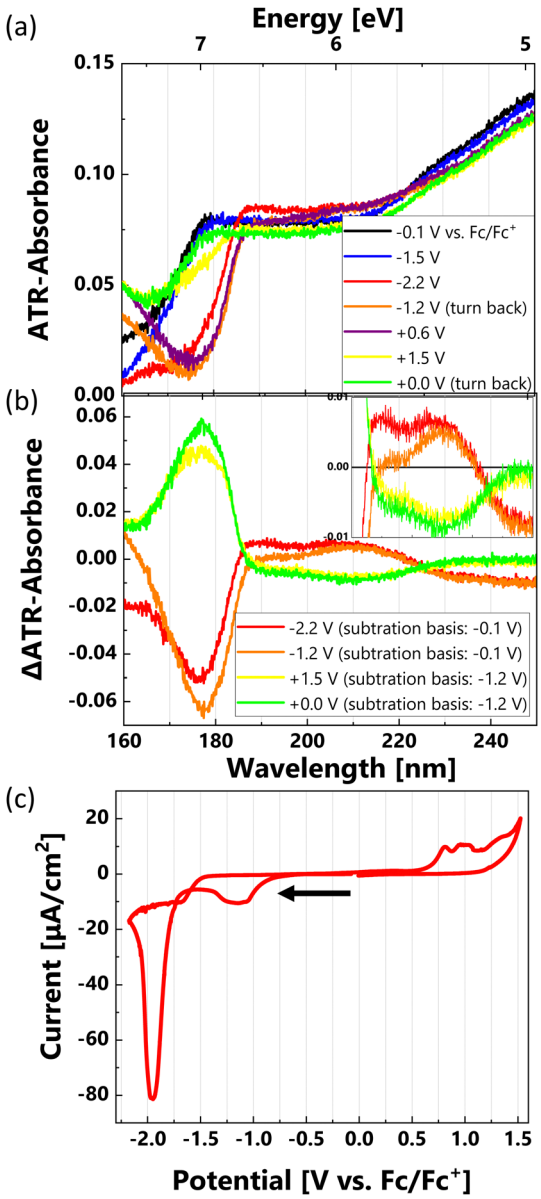

Fig. 5 (a) EC-ATR-FUV spectra of the interface in the LIL solution during the first cycle within the potential range of −2.2 to +1.5 V *vs.* Fc/Fc$^+$. (b) Difference spectra derived from (a), highlighting the changes in the interfacial composition, with an enlarged view of the 180–220 nm range shown in the inset. (c) Simultaneously measured CV curve.

at 0 V during the negative-going potential scan (Fig. 5(a)). Therefore, the key finding of these spectral measurements is that the spectrum change against the potential cycle was "reversible". Our focus was on elucidating the origin of this reversible phenomenon, which significantly differed from that observed in the neat IL.

The spectral change at the initial negative-going scan can be assumed to be linked to the partial decomposition of the EMIM cation. This assumption is supported by the observation of a reduction current peak at −1.9 V (Fig. 5(c)) and a decrease in EMIM cation absorption within the same potential range (Fig. 5(a)). However, in an independent experiment where the potential was maintained at −2.2 V *vs.* Fc/Fc$^+$, the reduction current greatly reduced in a few hundred seconds, while the decrease in EMIM cation absorption remained consistent. This observation suggests that the reduction in EMIM cation absorption is not solely caused by the breakdown of the interfacial EMIM, but rather by the quasi-equilibrium EDL structure influenced by the applied potential. The exact origin of the reduction current peak at −1.9 V *vs.* Fc/Fc$^+$ remains unclear. Potential explanations include the partial decomposition of EMIM and/or TFSI[29,30] or the underpotential deposition of Li$^+$ on the Au electrode.[31] The partial decomposition of the IL at the electrode interface may contribute to the formation of a thin solid layer known as the solid electrolyte interphase. However, the key observation is that the spectral changes throughout the potential cycle were "reversible" within the potential range of −2.2 to +1.5 V *vs.* Fc/Fc$^+$, as noted above. This suggests that the system reached a quasi-equilibrium state at these potentials, allowing us to focus on the changes in the EDL structure.

The decrease in the EMIM cation absorption at 176 nm and the increase in the TFSI absorption at 190–220 nm region at −2.2 V can be explained by the replacement of the EMIM cation with the Li$^+$ cation coordinated by TFSI anions. The small size of Li$^+$ (high density of positive charges) should result in stronger coordination with negatively charged TFSI anions. The coordination of TFSI anions in bulk liquids was analyzed using vibrational spectroscopy. Various types of TFSI coordination have been proposed based on experiments and calculations.[32–34] When considering the electrostatic interaction with the negative charge of the Au electrode surface, it is not clear whether the Li$^+$ coordinated with TFSI anions is more advantageous than the EMIM cation. A recent study on an MD simulation of Li$^+$ in an IL (*N*-methyl, *N*-propylpyrrolidinium bis(fluorosulfonyl)imide (C3mpyr-FSI)) reported that the adsorption energy of Li$^+$ coordinated by FSI anions became larger than that of C3mpyr cation on a Li metal surface when a high negative charge density (−14.4 μC cm^{-2}) was applied.[35] This is likely due to the large negative charge at the Li metal electrode surface deforming the local structure of FSI coordination to expose the Li$^+$ against the electrode. The TFSI absorption at 190–220 nm consists of some peaks (see the inset of Fig. 5(b)) and the difference in peak intensity may be linked to the coordination of Li$^+$. Our previous work has indicated that the changes in the coordination number of dicyanamide (DCA) anion with Li$^+$ can be captured as spectral changes in ATR-FUV.[36] However, calculating the absorbance of the deformed coordination, which may occur in a specific environment at the interface, proved challenging.

As shown in the spectra in Fig. 5, the EMIM cations are predominantly favored at the Au electrode surface within the potential range of −0.1 to −1.5 V *vs.* Fc/Fc$^+$. At the initial reversal potential of −2.2 V, a significant substitution of the EMIM cation with Li$^+$ cation, coordinated by TFSI anions, occurred and was maintained during the subsequent positive-going potential scan up to +0.6 V. Upon reaching the second reversal potential of +1.5 V, Li$^+$ cations, coordinated by the TFSI anions, were replaced by the EMIM cations, despite the positive charge on the Au electrode (the reverse process of the initial substitution).

Consistent changes were observed in the EC-ATR-IR spectrum of the interface. We selected the spectral range of 900–1500 cm^{-1}, where vibrational modes of $\nu_{as}(SO_2)$ (1320–1360 cm^{-1}), $\nu(CF_3)$ (1190–1240 cm^{-1}), $\nu_s(SO_2)$ (1130 cm^{-1}), and $\nu_a(SNS)$ (1060 cm^{-1}) for TFSI anions were detected.[33,37] Fig. 6(a) shows the selected difference spectra of EC-ATR-IR, focusing on the change around −2.0 V *vs.* Fc/Fc^+, where significant changes were observed by EC-ATR-FUV (Fig. 5). A spectrum at −1.8 V (subtraction basis: −0.1 V) in Fig. 6(a) during the negative-going potential scan from −0.1 V shows an increase in the absorption of all the vibrational bands mentioned above. This observation is consistent with the increase in the concentration of TFSI anion at the electrode interface. Upon reaching −2.2 V, the difference spectrum at −2.2 V (subtraction basis: −1.8 V) in Fig. 6(a) shows similar magnitude of absorptions for $\nu(CF_3)$ and $\nu_{as}(SO_2)$ indicating that the increase of absorption for these bands was similar for −1.8 V to −2.2 V. It can be noted that the increase in $\nu_{as}(SO_2)$ absorption was larger than the others.

Previous reports of MD calculations have shown that a TFSI anion coordinates with Li^+ through an oxygen atom of the negatively charged SO_2 moiety.[38] If Li^+ is attracted to the negatively charged Au electrode at −2.2 V by electrostatic forces, the TFSI anions coordinated to the Li^+ through the oxygen atom should rather be repelled from the negatively charged Au electrode. This deformation of the local structure and may align the dipole of $\nu_{as}(SO_2)$ more perpendicular to the electrode. Consequently, the inhomogeneously enhanced absorption could be attributed to the change in the coordination of TFSI anions to Li^+ upon approaching the Au electrode surface.

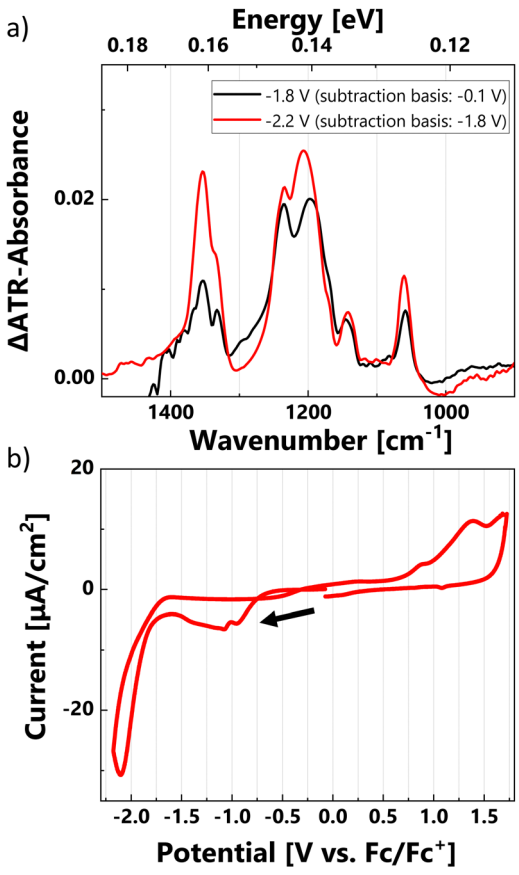

Fig. 6 (a) EC-ATR-IR spectra of the interface during the first cycle, the changes in IR absorbance across various potential ranges: differences from −0.1 V to −1.8 V (black line) and from −1.8 V to −2.2 V (red line) *vs.* Fc/Fc^+. (b) Simultaneously measured CV curve for the first cycle.

Origin of cathodic window enlargement

Finally, we discuss the potential origin of the extending the cathodic limit through the addition of Li-TFSI salt. As shown in Fig. 7, it was newly found that the presence of Li^+ cations in the system causes the EMIM cations to be repelled from the negatively charged Au electrode without undergoing significant decomposition. This occurs because the Li^+ ions, coordinated by TFSI anions, exhibits a higher priority to the Au electrode surface having high negative charge density by displacing the EMIM cations. The process of this displacement was effectively verified using interface-selective EC-ATR-FUV spectroscopy (Fig. 5) and supported by the results of EC-ATR-IR spectroscopy presented in Fig. 6. The EMIM cation possesses a lower unoccupied orbital and represents the most reactive component of the LIL electrolyte. The reduction in the quantity of EMIM cations at the electrode interface resulting from this displacement is expected to lead to a decreased rate of decomposition of EMIM cations on the electrode.

The approaching Li^+ ion coordinated by the TFSI anions is likely deformed or reduced in the number of coordinated TFSI anions (*i.e.*, desolvation), exposing Li^+ to electrostatic attraction from the negative charge on the Au electrode surface. In this configuration, the coordinated TFSI anions are repelled from the negative charge on the Au electrode surface, which may contribute to reducing the probability of the TFSI anion decomposition.

Conclusions

In this study, we analyzed the potential-dependent dynamic behaviors of cations and anions at the EMIM-TFSI IL (with and without Li^+ solute)/Au electrode interface by interface-selective spectroscopy of the EC-ATR-FUV method. In contrast to the typical behavior of TFSI anions being replaced by EMIM cations at the electrode interface observed in neat EMIM-TFSI, a significant replacement of the EMIM cation with Li^+ cation coordinated by TFSI anions was observed at the negatively charged Au electrode at −2.2 V *vs.* Fc/Fc^+. The reverse replacement occurred at +1.5 V, indicating a "reversible" cycle within

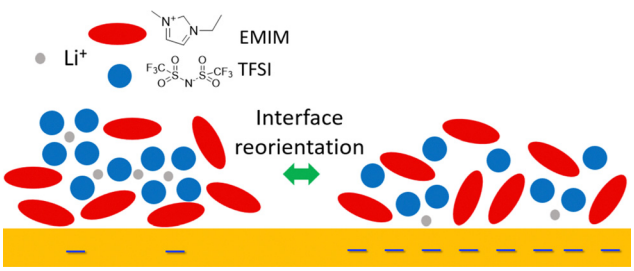

Fig. 7 Proposed schematic of the molecular behavior of LIL on a negatively charged electrode based on the present study.

the potential range of −2.2 to +1.5 V *vs.* Fc/Fc^+. This experimental evidence supports a concept which was partially proposed by simulation methods.

The surface-stabilized Li^+ coordinated by the TFSI anions limits the direct interaction of the EMIM cation with the electrode, thereby reducing the reduction rate of the EMIM cation. This restriction extends the cathodic limit in the LIL electrolyte. These findings offer valuable insights will give us an important insight into interface analysis in battery systems, with a focus on investigating a more realistic interface in our future research.

Author contributions

T. K. planned, conducted, analyzed, and summarized this study; I. T. and K. F. shared the methodology of the EC-ATR-FUV measurements and their analysis; I. A., S. K., I. T., and K. F. provided proper advice for conducting the research, interpreting the data, and writing the document; T. K. and K. F. is the representative author of this study.

Data availability

The data supporting this article have been included as part of the ESI.†

Conflicts of interest

There are no conflicts to declare.

Acknowledgements

This work was supported by JST, the establishment of university fellowships towards the creation of science technology innovation (grant number JPMJFS2125). This work was also supported by JSPS KAKENHI, grant numbers 19H02687 and 22H02049.

Notes and references

1 N. Kamaya, K. Homma, Y. Yamakawa, M. Hirayama, R. Kanno, M. Yonemura, T. Kamiyama, Y. Kato, S. Hama, K. Kawamoto and A. Mitsui, *Nat. Mater.*, 2011, **10**, 682.
2 Y. Yamada, K. Furukawa, K. Sodeyama, K. Kikuchi, M. Yaegashi, Y. Tateyama and A. Yamada, *J. Am. Chem. Soc.*, 2014, **136**, 5039.
3 M. Ishikawa, T. Sugimoto, M. Kikuta, E. Ishiko and M. Kono, *J. Power Sources*, 2006, **162**, 658.
4 M. Armand, F. Endres, D. R. MacFarlane, H. Ohno and B. Scrosati, *Nat. Mater.*, 2009, **8**, 621.
5 J. Lopes, M. Gomes and A. Padua, *J. Phys. Chem. B*, 2006, **110**, 16816.
6 Y. Yokota, T. Harada and K. Fukui, *Chem. Commun.*, 2010, **46**, 8627.
7 K. Fukui, *Bull. Chem. Soc. Jpn.*, 2018, **91**, 1210.
8 Y. Yokota, H. Miyamoto, A. Imanishi, K. Inagaki, Y. Morikawa and K. Fukui, *Phys. Chem. Chem. Phys.*, 2018, **20**, 6668.
9 H. Miyamoto, Y. Yokota, A. Imanishi, K. Inagaki, Y. Morikawa and K. Fukui, *Phys. Chem. Chem. Phys.*, 2018, **20**, 19408.
10 M. V. Fedorov and A. A. Kornyshev, *Chem. Rev.*, 2014, **114**, 2978.
11 R. Atkin, N. Borisenko, M. Druschler, S. Z. el-Abedin, F. Endres, R. Hayes, B. Huber and B. Roling, *Phys. Chem. Chem. Phys.*, 2011, **13**, 6849.
12 D. Okaue, I. Tanabe, S. Ono, K. Sakamoto, T. Sato, A. Imanishi, Y. Morikawa, J. Takeya and K. Fukui, *J. Phys. Chem. C*, 2020, **124**, 2543.
13 F. Greco, S. Shin, F. J. Williams, B. S. J. Heller, F. Maier and H. P. Steinruck, *ChemistryOpen*, 2019, **8**, 1365.
14 R. Wang, S. Bi, V. Presser and G. Feng, *Fluid Phase Equilib.*, 2018, **463**, 106.
15 K. Motobayashi and M. Osawa, *Electrochem. Commun.*, 2016, **65**, 14.
16 K. Motobayashi, K. Minami, N. Nishi, T. Sakka and M. Osawa, *J. Phys. Chem. Lett.*, 2013, **4**, 3110.
17 H. Matsumoto, H. Kageyama and Y. Miyazaki, *Electrochem.*, 2003, **71**, 1057.
18 V. Borgel, E. Markevich, D. Aurbach, G. Semrau and M. Schmidt, *J. Power Sources*, 2009, **189**, 331.
19 M. Yamagata, N. Nishigaki, S. Nishishita, Y. Matsui, T. Sugimoto, M. Kikuta, T. Higashizaki, M. Kono and M. Ishikawa, *Electrochim. Acta*, 2013, **110**, 181.
20 B. Dilasari, Y. Jung, G. Kim and K. Kwon, *ACS Sustainable Chem. Eng.*, 2015, **4**, 491.
21 M. Chen, J. Wu, T. Ye, J. Ye, C. Zhao, S. Bi, J. Yan, B. Mao and G. Feng, *Nat. Commun.*, 2020, **11**, 5809.
22 T. Iwahashi, Y. Miwa, W. Zhou, Y. Sakai, M. Yamagata, M. Ishikawa, D. Kim and Y. Ouchi, *Electrochem. Commun.*, 2016, **72**, 54.
23 N. Higashi, A. Ikehata and Y. Ozaki, *Rev. Sci. Instrum.*, 2007, **78**, 103107.
24 Y. Ozaki, Y. Morisawa and I. Tanabe, *Chem. Soc. Rev.*, 2024, **53**, 1730.
25 I. Tanabe, A. Suyama, T. Sato and K. Fukui, *Anal. Chem.*, 2019, **91**, 3436.
26 S. Kitano, I. Tanabe, N. Shioya, T. Hasegawa, T. Murata, Y. Morita, R. Tsuji and K. Fukui, *Langmuir*, 2023, **39**, 6846.
27 I. Tanabe, Y. Kurawaki, Y. Morisawa and Y. Ozaki, *Phys. Chem. Chem. Phys.*, 2016, **18**, 22526.
28 I. Tanabe, A. Suyama, T. Sato and K. Fukui, *Analyst*, 2018, **143**, 2539.
29 M. Tułodziecki, J. M. Tarascon, P. L. Taberna and C. Guéry, *Electrochem. Commun.*, 2017, **77**, 128.
30 N. De Vos, C. Maton and C. V. Stevens, *ChemElectroChem*, 2014, **1**, 1258.
31 L. H. Gasparotto, N. Borisenko, N. Bocchi, S. Z. El Abedin and F. Endres, *Phys. Chem. Chem. Phys.*, 2009, **11**, 11140.
32 T. Umecky, Y. Saito, Y. Okumura, S. Maeda and T. Sakai, *J. Phys. Chem. B*, 2008, **112**, 3357.
33 J. C. Lassegues, J. Grondin, C. Aupetit and P. Johansson, *J. Phys. Chem. A*, 2009, **113**, 305.
34 Z. Li, G. D. Smith and D. Bedrov, *J. Phys. Chem. B*, 2012, **116**, 12801.

35 U. Pal, D. Rakov, B. Lu, B. Sayahpour, F. Chen, B. Roy, D. R. MacFarlane, M. Armand, P. C. Howlett, Y. S. Meng and M. Forsyth, *Energy Environ. Sci.*, 2022, **15**, 1907.
36 M. Imai, I. Tanabe, A. Ikehata, Y. Ozaki and K. Fukui, *Phys. Chem. Chem. Phys.*, 2020, **22**, 21768.
37 M. Herstedt, M. Smirnov, P. Johansson, M. Chami, J. Grondin, L. Servant and J. C. Lassègues, *J. Raman Spectrosc.*, 2005, **36**, 762.
38 V. Lesch, Z. Li, D. Bedrov, O. Borodin and A. Heuer, *Phys. Chem. Chem. Phys.*, 2016, **18**, 382.